ACS Photonics

Letter

Cite This: ACS Photonics 2018, 5, 1839−1845

All-Polymer Integrated Optical Resonators by Roll-to-Roll Nanoimprint Lithography

Anna V. Shneidman,*[,†,‡] Kaitlyn P. Becker,[†,‡,§] Michael A. Lukas,[§] Nicholas Torgerson,[§] Cheng Wang,[‡] Orad Reshef,[‡] Michael J. Burek,[‡] Kateri Paul,[§] Joseph McLellan,*[,§] and Marko Lončar*[,‡]

[‡]John A. Paulson School of Engineering and Applied Sciences, Harvard University, 29 Oxford Street, Cambridge, Massachusetts 02138, United States

[§]Nano Terra, Inc., 737 Concord Avenue, Cambridge, Massachusetts 02138, United States

ABSTRACT: Polymers are a highly versatile class of materials for micro and nanofabrication. They have been studied for applications in photonics as they can be readily processed, integrated, and doped with a wide range of materials, and can be flexible and stretchable, providing numerous opportunities such as wearable devices and structures with tunable photonic response. Roll-to-roll nanoimprint lithography (R2RNIL) is a method to produce all-polymer devices, which provides the opportunity to target applications where low cost and high throughput are needed most. Here, finite difference time domain simulations are performed to determine the requirements for R2RNIL in order to produce functional photonic integrated circuits. A wide range of nanophotonic devices are fabricated, including waveguides, photonic crystals, diffraction gratings, and ring resonators. Loaded quality factors as high as 57500 are measured in ring resonators at the telecom wavelength range, enabling on-chip high resolution sensors and spectrometers.

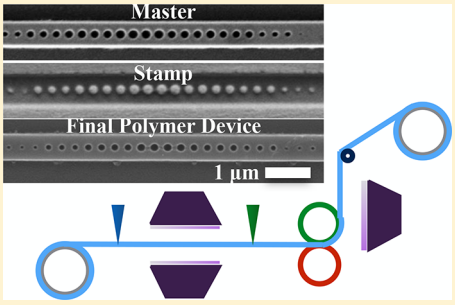

KEYWORDS: *polymer photonics, roll-to-roll nanoimprint lithography, photonic integrated circuits, microring resonators, ridge waveguides*

Roll-to-roll (R2R) fabrication is a ubiquitous technique in manufacturing applications requiring continuous and high-throughput production. With the advent of nanometer to micron scale molding techniques,[1] integrated micro- and optoelectronics produced by R2R nanoimprint lithography (NIL) fabrication are finding prevalence in many disciplines, including flexible electronics,[2] photovoltaics,[3] and display technologies,[4] thus helping to bridge the ever-present gap between academic research and real-world applications. Importantly, R2RNIL provides an opportunity to use polymers, which are leading material candidates for applications requiring inexpensive, high-throughput fabrication, such as point-of-care (POC) medical diagnostics and food and water safety monitoring in developing countries.[5] Polymers have many additional advantageous characteristics for photonics; they are readily deposited on a wide variety of substrates and on curved surfaces,[6] and they can be tailored through chemistry during synthesis or postmodification to achieve desired physical or chemical properties such as refractive index profile, thermal response, hydrophilicity, reactivity, and dopant inclusions.[7,8]

In this Letter, we demonstrate on-chip all-polymer photonic integrated circuits (PICs) by high-throughput and cost-effective R2RNIL manufacturing. PICs are important for a broad range of disciplines and industries, for example, giving access to novel physics in quantum[9] and nonlinear optics,[10,11] as well as serving as excellent sensors for environmental or biomedical analysis.[12] Applications that demand ultrahigh sensitivity and small on-chip footprints, such as medical and environmental sensing, often rely on structures that provide high confinement of electromagnetic fields for high frequency resolution (e.g., for on-chip spectrometers) or strong interactions with analytes (e.g., direct sensors). To this aim, together with the motivation for low cost, NIL has been previously employed to produce all-polymer integrated ring resonators.[13−15] Here we demonstrate an important step toward mass production, presenting all-polymer ring resonators fabricated by R2RNIL, with a measured loaded optical quality (Q) factor of approximately 57500 for wavelengths between 1480 and 1680 nm, enabling a frequency resolution of ∼25 picometers. The material choice is first discussed, followed by optical simulations conducted to determine the geometries that support light propagation and to guide the R2RNIL design to be able to achieve the geometric requirements. The fabrication to produce a variety of components for on-chip photonics and optical transmission measurements are presented.

The polymers employed for the photonic structures were UV-curable Norland Optical Adhesives (NOAs; Norland Products, Inc.),[16] selected for their relatively low cost, $300-$400 per pound, and wide transparency window, as broad as 400 nm to 2 μm. A variety of NOAs are available, featuring a

Received: January 5, 2018
Published: April 17, 2018

DOI: 10.1021/acsphotonics.8b00022
ACS Photonics 2018, 5, 1839−1845

large range of refractive indices, from n = 1.315 (NOA 1315) to n = 1.64 (NOA 164), making it possible to select polymers with a sufficiently high refractive index contrast for on-chip electromagnetic field confinement and guiding, and an extensive range of viscosities (10−5000 cps), important for achieving the desired speed of replication and molding thickness. In this work, we chose NOA 13685 (n = 1.3685, viscosity at room temperature 200 cps, curing wavelength 315−400 nm) to form the upper and lower cladding layers and NOA 71 (n = 1.56, viscosity at room temperature 15−25 cps, curing wavelength 315−395 nm) for the core layer of the photonic structures.

NIL presents a challenge toward PIC fabrication, as the process leaves an unavoidable residual layer, known as the "pedestal", between the molded structure and the substrate (Figure 1a),[17] so that the propagating electromagnetic field

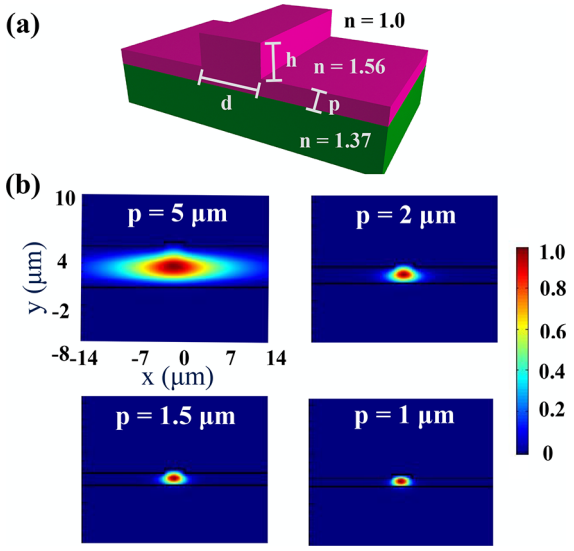

Figure 1. Ridge waveguide modes for progressively thinner pedestals. (a) Schematic illustrating the ridge waveguide cross-section that results from NIL. (b) Energy distribution for the electromagnetic field of the fundamental mode for rib waveguides of different cross sections. In all cases, d and h are fixed at 3.2 and 1 μm, respectively, while p is indicated on the corresponding plot. The color bar indicates the distribution of electromagnetic energy contained in the fundamental transverse electric (TE) mode; the mode distribution and trend with increasing pedestal thickness are similar for the fundamental transverse magnetic (TM) mode. x and y axes are the same for all plots.

preferentially leaks into the pedestal, preventing the optical confinement necessary for low-loss waveguiding (most evident in Figure 1b, where the pedestal thickness is 5 μm). Fortunately, the pedestal thickness can be substantially reduced by selecting the appropriate combination of molding parameters, including the initial thickness of the liquid polymer, its viscosity, the pressure during the UV curing, and the molding velocity.[18−21] In order to specify the requirements for the R2RNIL system, we conducted optical simulations to determine the pedestal thicknesses that would allow for adequate mode confinement for a ridge waveguide comprising NOA 1368 as the bottom cladding, NOA71 as the molded device layer, and exposed to air on top (cross-section depicted in Figure 1a). The electromagnetic field profiles of the guided modes were computed using a commercial eigenmode solver (*MODE Solutions*; Lumerical, Inc.). The waveguide width and height were fixed to d = 3.2 μm and h = 1 μm, respectively, to minimize the number of modes supported by the structure while maintaining negligible bending losses, as determined by simulation for large (1 mm) bending radii. The pedestal thickness p was varied in simulations, indicating that mode confinement to the ridge is possible for the chosen d and h when $p \leq 1$ μm (Figure 1b).

The R2RNIL tool (Figure 2) was designed to accommodate the requirement for submicron pedestal thickness in order to be able to produce structures with the optical confinement essential for routing the light on chip and achieving high Q-factor optical resonators. We employed pneumatic cylinders (5.08 cm wide, 5.08 cm diameter) and rollers that could supply and sustain the high pressures required to squeeze out excess liquid polymer to reduce the pedestal thickness, applying up to 600 lbs of force to the molding interface between the stamp and Teflon roller in this case. A rerouting roller positioned above the stamp roller held the web in contact with the back of the stamp roller, onto which a 600 W UV flood lamp (Uvitron SUN-RAY 600 SM UV) was positioned for curing so that the molded polymer was cured through the web before it was peeled away from the stamp roller.

The full fabrication process is depicted in Figure 2 and presented in detail in the Experimental Section. Briefly, we first fabricated a master mold in a silicon wafer by defining the photonic structures with electron beam lithography (EBL; ELS-F125, Elionix, Inc.), followed by reactive ion etching with an inductively coupled plasma (C_4F_8/SF_6, RIE-ICP; STS MPX/LPX). We used the Si master as a mold for the UV-curable polymer perfluoropolyether (PFPE Sartomer CN5001; Arkema, Inc.) to prepare the working stamp, containing the inverse of the final structures (Figure 2a). We selected PFPE as the stamp material for integration into the R2R system due to its favorable characteristics, including high resolution reproduction of photonic structures, flexibility, and low surface energy.[22] The stamp was attached to the curved surface of the molding roller in the R2R machine. Once a stamp became fouled (approximately after 40 replica cycles), a new stamp could be prepared from the same master, as the master exhibited no evidence of deterioration in quality.

The cladding polymer NOA 13685 was first dispensed in liquid form onto the flexible film, known as the web, which wound between the rollers and supported the polymers throughout the molding and cladding processes (Figure 2b). We selected a 2 in. wide (5.08 cm), 0.005 in. (127 μm) thick polyethylene terphthalate (PET; Grax Dura-Lar) plastic film as the web material because of its sturdiness, flexibility, ease of availability, and sufficient transparency to the curing wavelength. The PET web originated at the source spool and was drawn through the various stages of the tool by the collection spool on the far right. The source and collection spools were both equipped with concentric torque limiting shaft couplings (McMaster 9132K11) to maintain tension on the web, keeping it flat throughout the molding process. Since NOA 13685 curing is inhibited by oxygen, nitrogen was flowed in the vicinity of the curing process. After curing a thick (~10 μm) layer of NOA 13685 between two UV lamps, NOA 71 was dispensed onto the web and cured while pressed against the stamp roller with a high force to eliminate as much of the residual, pedestal-forming liquid. Once molding was complete, we removed the web from the collection spool and cut the devices for optical measurements.

DOI: 10.1021/acsphotonics.8b00022
ACS Photonics 2018, 5, 1839−1845

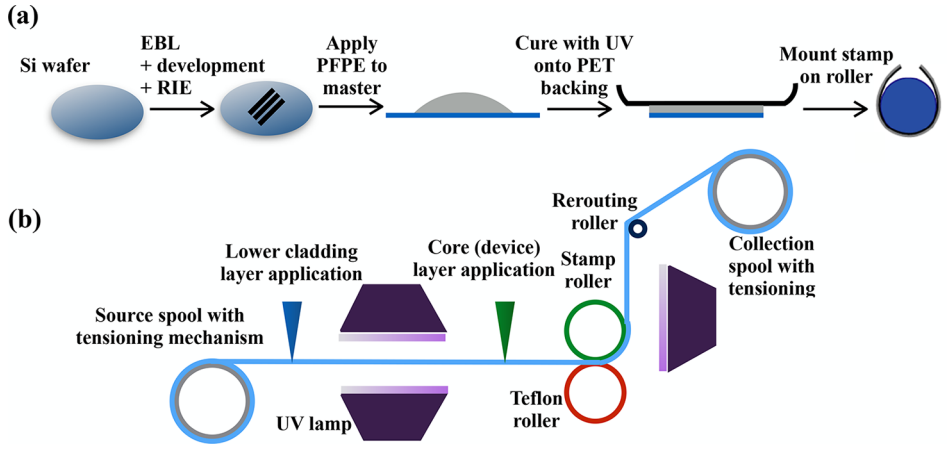

Figure 2. Process flow for roll-to-roll nanoimprint lithography (R2RNIL). (a) Schematic of the process flow. A master is created in silicon using electron beam lithography (EBL) and reactive ion etching (RIE), from which a stamp is prepared in perfluoropolyether (PFPE) and mounted onto a roller in the R2RNIL machine. (b) Schematic of the basic anatomy of the R2RNIL tool, consisting of rollers around which the polyethylene terphthalate (PET) web is wound and UV lamps for curing the NOA material. The stamp and Teflon rollers are attached to pistons so that high pressures can be applied to promote the liquid NOA to fill the grooves of the stamp.

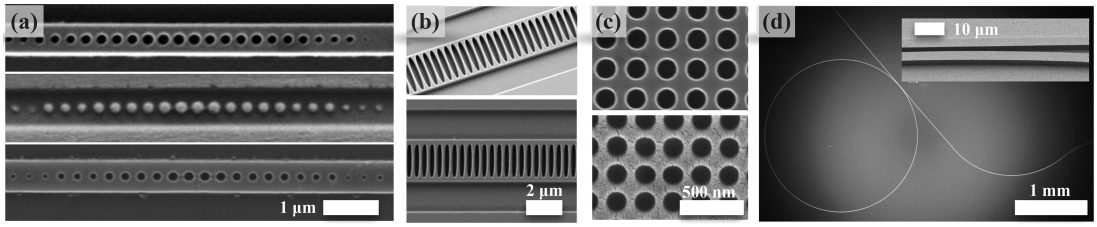

Figure 3. Variety of structures fabricated by the R2RNIL method. SEM images of (a) master (top), stamp (middle), and replica (bottom) for a 1D nanobeam photonic crystal cavity (the waveguide width and height are 700 and 220 nm, respectively, the pitch is 300 nm, and the hole diameter decreases from 165 nm at the center to 80 nm at both ends); (b) master (top) and replica (bottom) of a 1D nanobeam photonic crystal cavity with elliptical holes (3.2 μm wide and 500 nm tall waveguide, pitch was 550 nm, ellipse minor and major axes linearly decrease from the center to both ends from 165 to 140 nm, and from 1.44 to 1.22 μm, respectively); (c) master (top) and replica (bottom) of a portion of a photonic crystal slab featuring 100 × 100 array of holes with 100 nm radii, 700 nm center-to-center distance, and approximately 90 nm hole depth; (d) master of a 1 mm ring resonator coupled to an s-shaped waveguide (3.2 μm wide, 1.5 μm tall) via a 1.2 μm coupling gap (inset, SEM of the coupling region in the replica coated with 10 nm of 80:20 Pt:Pd to prevent charging).

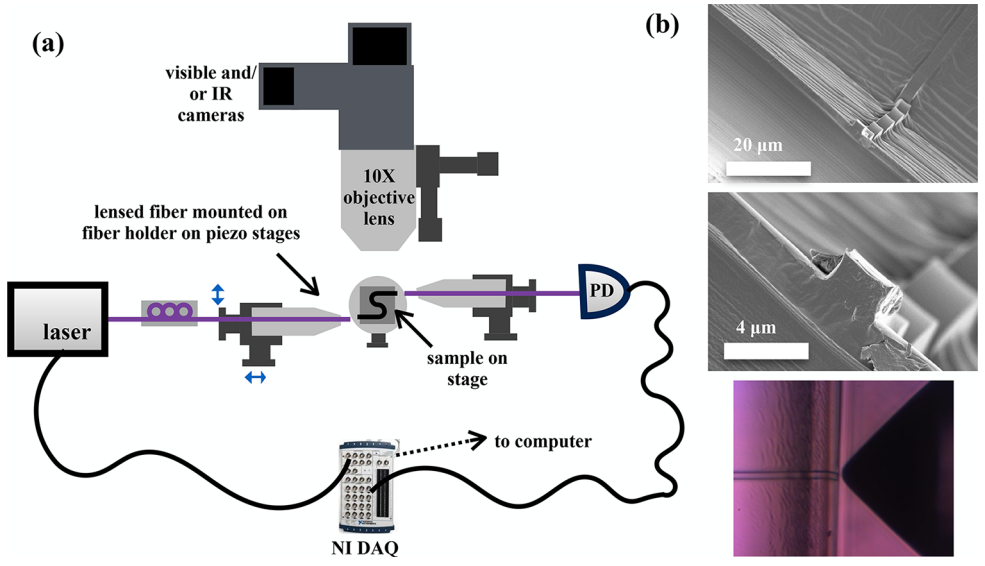

Figure 4. Optical transmission measurement setup. (a) Schematic of the measurement setup. The hollow tube contains a focusing lens to focus the light onto the camera(s), a beamsplitter in case two cameras are used, and a zoom lens. FPC = fiber polarization control, PD = photodiode, NI-DAQ = National Instrument Data Acquisition. (b) SEM images of the waveguide facet cut by a razor blade (top), zoom-in to the facet (middle), and a photograph of a lensed telecom fiber coupled to one side of the waveguide of a device-under-test (bottom).

DOI: 10.1021/acsphotonics.8b00022
ACS Photonics 2018, 5, 1839−1845

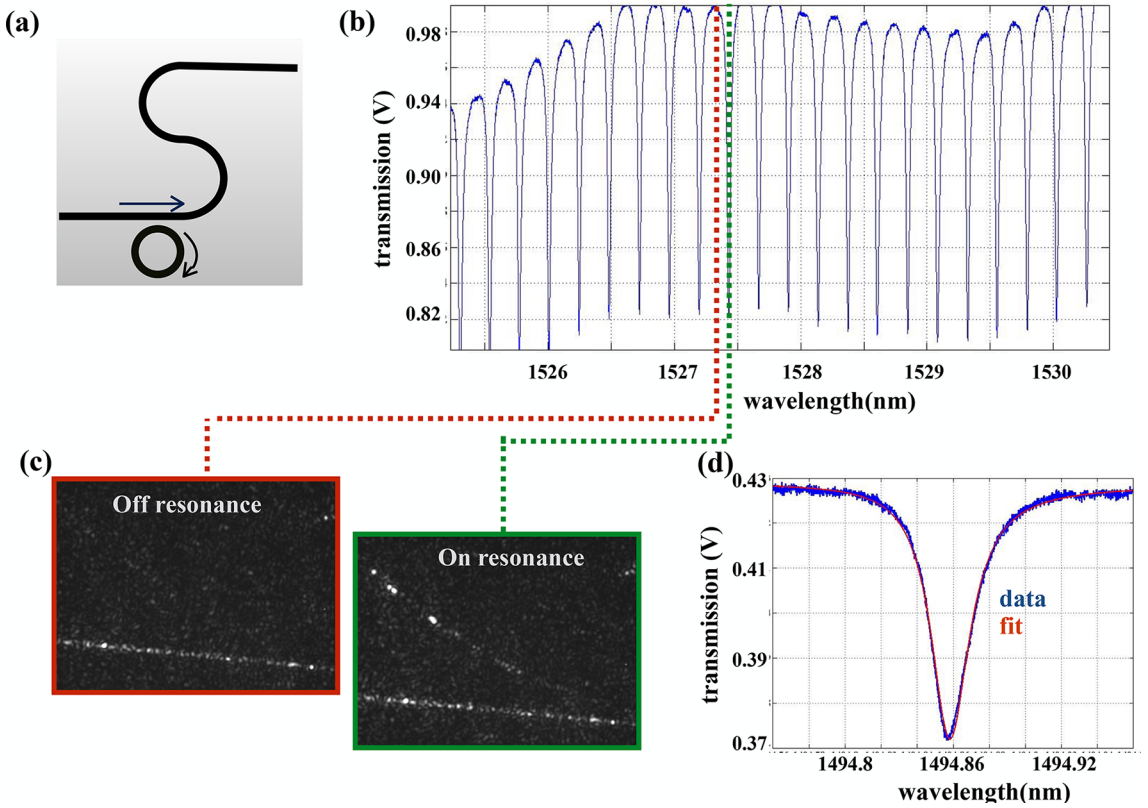

Figure 5. Optical transmission measurements. (a) Cartoon of the full device, consisting of a ring coupled to an s-waveguide. (b) Transmission measurement at telecom wavelengths, showing dips in transmission due to ring resonances. (d) Images taken with an IR camera when the laser wavelength is fixed either off resonance (red border), where scattering is seen from the waveguide only, not from the ring, or on resonance (green border), where scattering is seen both from the waveguide and the ring. (d) High resolution scan of one resonance dip. Q from fit: 57500 ± 200.

As shown in the SEM images in Figure 3, all-polymer replicas of a variety of photonic structures were achieved, all of which demonstrated good fidelity to the master mold dimensions, a broad range of feature sizes ranging from below 100 nm to several millimeters, and reproduction over large areas (e.g., 100 cm^2, limited here by the width of the web, the size of rollers, and the area over which the piston could apply a uniform pressure, but could be extended by orders of magnitude in an industrial setting); the minimum reproducible feature size of 100 nm is a result of the resolution of the initial lithography used to create the master as well the capillary forces, which dictate the filling of the small features by the chosen polymer in its liquid form.[23]

One type of replicated structure was the nanobeam photonic crystal cavity (Figure 3a,b), based on those previously produced using EBL and RIE in different material platforms including silicon-on-insulator and EBL resists, and for which excellent sensing results have been demonstrated for biological and chemical analytes.[24,25] As shown in the SEM images in Figure 2a, the all-polymer replica nanobeam photonic crystals contained holes below 80 nm in diameter together with waveguides that were up to 500 nm wide and centimeters long. We also replicated structures previously employed for applications in optomechanics,[26,27] consisting of 2D arrays of holes (Figure 2c) as well as their inverse, consisting of pillars. These replica molded structures displayed angle-dependent color which can be used toward display technologies or colorimetric sensing.[28−30] Ring resonators coupled to waveguides featuring micron-scale distances between the rings and waveguides spanning centimeters in length (Figure 3d) were also reproduced, as well as isolated and connected trenches and ridges ranging in width from 100s of nanometers to 100s of microns. All of these structures can be replicated together in a single R2RNIL run.

Transmission measurements were obtained for a polymer ring resonator coupled to an s-shaped waveguide (Figure 3d, SEM) as a representative integrated photonic structure produced by R2RNIL. We used a typical end-fire coupling[31] setup (Figure 4a) employing lensed single mode SMF-28 fibers (OZ Optics, Ltd.). In order to couple laser light on and off chip, we sliced both ends of the waveguide with a razor blade and approached the lensed fibers to either end using motorized stages. The fiber at one edge of the chip focused laser light in the telecom C- and L-Band wavelength range (1480−1680 nm) from a tunable continuous wave laser (Santec TSL-510) onto one waveguide facet, while a second lensed fiber at the opposing edge collected the transmitted light from the exit waveguide facet and delivered it to an InGaAs photodetector (Newport 1811). As shown in the SEM images of Figure 4b, the exposed end facets can exhibit buckling due to shear forces induced during the cutting process; this contributes to insertion losses and can potentially be eliminated by employing different cutting methods or tools, for example, slicing with a sharper blade, clamping the materials during cutting, using laser cutting, or performing ion beam milling.

The measured device is depicted schematically in Figure 5a. The waveguide width, height, and pedestal thickness for the device under test were measured from the SEM images to be $d \approx 3.2\ \mu m$, $h \approx 1\ \mu m$ and $p \approx 1\ \mu m$, respectively, and the coupling gap (shortest distance between the ring and

DOI: 10.1021/acsphotonics.8b00022
ACS Photonics 2018, 5, 1839−1845

waveguide) was 1.2 μm. We set the bending radii to 1 mm in order to minimize bending losses. The s-shape was chosen to ensure that the measured transmission signal was due to laser light guided through the fabricated ridge waveguide, rather than guiding through the pedestal as a slab mode or scattering from the input to output fiber. The measured transmission spectrum is shown in Figure 5b. Dips in the transmission spectrum correspond to resonance wavelengths supported by the ring resonator. We further confirmed this through images captured with an infrared camera placed above the optical chip: when the input laser wavelength was fixed on resonance, scattering out of the ring was observed in the camera image, while no scattering from the ring resonator was observed with the laser tuned off resonance (Figure 5c). For a ring with radius R and, thus, total path length $L = 2\pi R$, the distance between resonances, the free spectral range (FSR), is expected to be

$$\mathrm{FSR} = \frac{\lambda^2}{n_g L} \tag{1}$$

at an operational wavelength of λ and a group index of n_g.[32] For the rings measured here, R = 1 mm, $\lambda \approx$ 1550 nm, and n_g = 1.593 was obtained from frequency analysis with *MODE Solutions*. The expected FSR is thus 0.24 nm, in close agreement with the experimentally extracted value of 0.23 nm ± 0.005.

The loaded optical Q-factor of these resonances, defined as the center wavelength divided by the full width at half minimum (fwhm) of a transmission dip, is a key parameter for spectroscopy and sensing, as it determines both the frequency resolution and sensitivity of the device. It is extracted from the transmission measurements by fitting a Lorentzian line shape to the transmission dips. Figure 5d depicts such a fit to an example transmission dip, which gives Q = 57500 ± 200 and corresponds to a spectral resolution of approximately $\Delta\lambda = \lambda/Q \approx$ 1495 nm/57500 = 26 pm. This sets an upper bound on the losses of $2\pi n_g/(\lambda Q) = 2\pi$*1.593/(1495*10^{-7} cm*57500) ≈ 5.06 dB/cm,[33,34] and is comparable to what has been demonstrated in other photonic integrated platforms based in polymer.[35−38] We note that 5 dB/cm is a conservative estimate, and could be much lower when coupling losses are taken into account. The reported high Q factor and corresponding low propagation loss validate our choice of polymer and method of fabrication.

In summary, we have established a R2RNIL tool for the fabrication of all-polymer on-chip photonic devices, with feature sizes ranging from below 100 nm up to several millimeters. Since the silicon master can be used almost indefinitely (no fouling or reduction of performance was observed for thousands of device replicas), the costs of EBL and RIE used to produce it are negligible compared to the material (polymers used for cladding and core and the web) costs. Assuming that a single stamp can be reliably replicated 40× before fouling, consistent with experimental observations, and taking into account the total volume of material used to make the device as well as the excess material, which is inevitable for the fabrication process, we obtain an estimated cost of $0.01 per square centimeter. We demonstrated and characterized all-polymer integrated optical ring resonators prepared by the R2R method. The total Q-factor was extracted from a fit to the transmission spectrum, revealing excellent material properties, enabling a variety of fundamental studies and industrial applications. An array of resonant devices could be used as low-cost on-chip spectrometers for highly sensitive analyte detection which would pave the way to better, more accessible diagnostics, especially in developing countries thanks to the low cost and scalability of the R2R technique. We envision that polymer photonic structures produced by R2RNIL will also be used toward integrated on-chip quantum and nonlinear circuits, with the possibility to incorporate other materials such as emitters and absorbers for light sources, detectors, and other applications.[39]

EXPERIMENTAL SECTION

Roll-to-Roll Nano Imprint Lithography. The speed and tension with which the collection spool pulls the web can be adjusted with a power supply connected to the motor driving the assembly and a variable spring-loaded clutch. Between the source and the collection spool, the R2R process consists of two steps: (1) a 10 μm thick layer of NOA 13685 is applied to the PET web and UV-cured to form the lower cladding and (2) NOA 71 is imprinted on top of the cladding to create the device layer. For all steps, NOA is deposited in liquid form onto the PET web using a syringe pump (KD Scientific). The syringe pump sets supply flow at a controlled rate to accommodate the desired layer thickness and web velocity. The uncured polymer for the lower cladding layer is spread over the width of the web using a doctor blade positioned by two micrometer heads. After exiting the doctor blade, the cladding is cured between two UV flood lamps (Caution! UV shielding must be used). NOA 71 is then deposited on top of the lower cladding layer and passed through a pair of rollers that squeeze the uncured polymer to a submicron thickness with the help of four pneumatic cylinders. The upper roller, covered by the PFPE stamp that contains the inverse of the final structure, is pressed into the uncured polymer. The lower roller is covered with a thin sheet of Teflon. After the web passes through the line of contact between the rollers, it is held in contact with the stamp clad upper roller and cured by another UV lamp (Caution! UV shielding must be used) directed to the backside of the upper roller. Once the NOA 71 is cured by the UV lamp, the replica-molded device is released from the stamp, transported by the web, and wound onto the collection spool from which it can later be removed and cut into segments for optical measurements. While it was not implemented in this tool, a third step to apply an upper cladding layer is an option using a process similar to the one used to add the lower cladding, as described above.

Optical Transmission Measurements. We collected transmission measurements at telecom wavelengths using lensed fiber coupling to the exposed on-chip waveguide facets. The lensed fibers were purchased from Oz-Optics and spliced into the optical setup. The fibers were approached to either end of the chip using motorized stages with 50 nm encoder precision. One fiber functioned as the input, delivering light from a Santec telecom laser, while the other fiber was used to collect the transmission and deliver it to the photodetector. A data acquisition (DAQ) board from National Instruments (NI) converted the analog voltage output from the photodiode to a digital signal. The DAQ was also used to synchronize the timing of readout from the photodetector with the change in frequency of the tunable Santec laser.

AUTHOR INFORMATION

Corresponding Authors

*E-mail: ashneidm@gmail.com.

DOI: 10.1021/acsphotonics.8b00022
ACS Photonics 2018, 5, 1839−1845

*E-mail: loncar@seas.harvard.edu.
*E-mail: jmclellan@nanoterra.com.

ORCID

Anna V. Shneidman: 0000-0001-6064-5378
Cheng Wang: 0000-0002-1939-1422
Orad Reshef: 0000-0001-9818-8491

Author Contributions

†These authors contributed equally to this work.

Notes

The authors declare no competing financial interest.

■ ACKNOWLEDGMENTS

This work was performed in part at the Harvard University Center for Nanoscale Systems (CNS), a member of the National Nanotechnology Coordinated Infrastructure Network (NNCI), which is supported by the National Science Foundation under NSF ECCS Award No. 1541959. CNS is part of Harvard University. Support was provided by DARPA SBIR Grant, Contract No. D12PC00356. The authors would also like to thank Pui-Chuen Hui, Vivek Venkataraman, Stefan Kalchmair, Parag Deotare, Nikolaj K. Mandsberg, and Qimin Quan for helpful discussions.

■ REFERENCES

(1) Chou, S. Y.; Krauss, P. R.; Renstrom, P. J. Imprint lithography with 25-nanometer resolution. *Science* **1996**, *272*, 85.
(2) Hu, L.; Wu, H.; La Mantia, F.; Yang, Y.; Cui, Y. Thin, flexible secondary Li-ion paper batteries. *ACS Nano* **2010**, *4*, 5843−5848.
(3) Krebs, F. C.; Tromholt, T.; Jørgensen, M. Upscaling of polymer solar cell fabrication using full roll-to-roll processing. *Nanoscale* **2010**, *2*, 873−886.
(4) Crawford, G. P.; Gregg, A.; York, L.; Strnad, M. In *Flexible Flat Panel Displays*; Crawford, G. P., Ed; John Wiley & Sons, Ltd: Chichester, U.K., 2005; pp 409−445.
(5) Yager, P.; Domingo, G. J.; Gerdes, J. Point-of-care diagnostics for global health. *Annu. Rev. Biomed. Eng.* **2008**, *10*, 107−144.
(6) Chen, R. T. Polymer-based photonic integrated circuits. *Opt. Laser Technol.* **1993**, *25*, 347−365.
(7) Ma, H.; Jen, A. Y.; Dalton, L. R. Polymer-based optical waveguides: materials, processing, and devices. *Adv. Mater.* **2002**, *14*, 1339−1365.
(8) Eldada, L.; Shacklette, L. W. Advances in polymer integrated optics. *IEEE J. Sel. Top. Quantum Electron.* **2000**, *6*, 54−68.
(9) Dietrich, C. P.; Fiore, A.; Thompson, M. G.; Kamp, M.; Höfling, S. GaAs integrated quantum photonics: Towards compact and multi-functional quantum photonic integrated circuits. *Laser Photonics Rev.* **2016**, *10*, 870−894.
(10) Silverstone, J. W.; Bonneau, D.; Ohira, K.; Suzuki, N.; Yoshida, H.; Iizuka, N.; Ezaki, M.; Natarajan, C. M.; Tanner, M. G.; Hadfield, R. H.; Zwiller, V.; Marshall, G. D.; Rarity, J. G.; O'Brien, J. L.; Thompson, M. G. On-chip quantum interference between silicon photon-pair sources. *Nat. Photonics* **2014**, *8*, 104−108.
(11) Foster, M. A.; Turner, A. C.; Sharping, J. E.; Schmidt, B. S.; Lipson, M.; Gaeta, A. L. Broad-band optical parametric gain on a silicon photonic chip. *Nature* **2006**, *441*, 960−963.
(12) Passaro, V.; Tullio, C. D.; Troia, B.; Notte, M. L.; Giannoccaro, G.; Leonardis, F. D. Recent advances in integrated photonic sensors. *Sensors* **2012**, *12*, 15558−15598.
(13) Huang, Y.; Paloczi, G. T.; Scheuer, J.; Amnon, Y. Soft Lithography Replication of Polymeric Microring Optical Resonators. *Opt. Express* **2003**, *11* (20), 2452−2458.
(14) Salleh, M. H. M.; Glidle, A.; Sorel, M.; Reboud, J.; Cooper, J. M. Polymer Dual Ring Resonators for Label-Free Optical Biosensing Using Microfluidics. *Chem. Commun.* **2013**, *49* (30), 3095.
(15) Morarescu, R.; Pal, P. K.; Han, X.; Zhao, M.; Bienstman, P.; Morthier, G. Polymer Microring Resonators for Biosensing Applications by Nanoimprint Lithography. *Transparent Optical Networks (ICTON), 2015 17th International Conference*; IEEE, 2015; pp 1−4.
(16) Norland Products Inc. Norland Optical Adhesives, https://www.norlandprod.com/adhesiveindex2.html (accessed Dec 2017).
(17) Paloczi, G. T.; Huang, Y.; Yariv, A.; Luo, J.; Jen, A. K. Y. Replica-molded electro-optic polymer Mach−Zehnder modulator. *Appl. Phys. Lett.* **2004**, *85*, 1662−1664.
(18) Lee, H.; Jung, G. Y. UV curing nanoimprint lithography for uniform layers and minimized residual layers. *Jpn. J. Appl. Phys.* **2004**, *43*, 8369.
(19) Guo, L. J. Nanoimprint lithography: methods and material requirements. *Adv. Mater.* **2007**, *19* (4), 495−513.
(20) Ahn, S. H.; Guo, L. J. High-speed roll-to-roll nanoimprint lithography on flexible plastic substrates. *Adv. Mater.* **2008**, *20*, 2044−2049.
(21) Aikio, S.; Hiltunen, J.; Hiitola-Keinänen, J.; Hiltunen, M.; Kontturi, V.; Siitonen, S.; Puustinen, J.; Karioja, P. Disposable photonic integrated circuits for evanescent wave sensors by ultra-high volume roll-to-roll method. *Opt. Express* **2016**, *24*, 2527−2541.
(22) Truong, T. T.; Lin, R.; Jeon, S.; Lee, H. H.; Maria, J.; Gaur, A.; Hua, F.; Meinel, I.; Rogers, J. A. Soft lithography using acryloxy perfluoropolyether composite stamps. *Langmuir* **2007**, *23*, 2898−2905.
(23) Lan, H.; Ding, Y. In *Nanoimprint Lithography in Lithography* [Online]; Wang, M., Ed.; InTech: Weinheim, Germany, 2010; Ch. 23 (accessed Dec 26, 2017) https://www.intechopen.com/books/lithography/nanoimprint-lithography.
(24) Quan, Q.; Floyd, D. L.; Burgess, I. B.; Deotare, P. B.; Frank, I. W.; Tang, S. K.; Ilic, R.; Loncar, M. Single particle detection in CMOS compatible photonic crystal nanobeam cavities. *Opt. Express* **2013**, *21*, 32225−32233.
(25) Deotare, P. B.; Kogos, L. C.; Bulu, I.; Lončar, M. Photonic crystal nanobeam cavities for tunable filter and router applications. *IEEE J. Sel. Top. Quantum Electron.* **2013**, *19*, 3600210−3600210.
(26) Hui, P. C.; Woolf, D.; Iwase, E.; Sohn, Y. I.; Ramos, D.; Khan, M.; Rodriguez, A. W.; Johnson, S. G.; Capasso, F.; Loncar, M. Optical bistability with a repulsive optical force in coupled silicon photonic crystal membranes. *Appl. Phys. Lett.* **2013**, *103*, 021102.
(27) Iwase, E.; Hui, P. C.; Woolf, D.; Rodriguez, A. W.; Johnson, S. G.; Capasso, F.; Lončar, M. Control of buckling in large micro-membranes using engineered support structures. *J. Micromech. Microeng.* **2012**, *22*, 065028.
(28) Liu, W.; Liu, X.; Yang, B. Photonic Crystals Fabricated via Facile Methods and Their Applications. In *Photonic Materials for Sensing, Biosensing and Display Devices*; Serpe, M. J., Kang, Y., Zhang, Q. M., Eds.; Springer International Publishing: Switzerland, 2016; pp 101−158.
(29) Lifson, M. A.; Miller, B. L. Photonic Crystals as Robust Label-Free Biosensors. In *Photonic Materials for Sensing, Biosensing and Display Devices*; Serpe, M. J., Kang, Y., Zhang, Q. M., Eds.; Springer International Publishing: Switzerland, 2016; pp 189−207.
(30) Cho, E. H.; Kim, H. S.; Cheong, B. H.; Oleg, P.; Xianyua, W.; Sohn, J. S.; Ma, D. J.; Choi, H. Y.; Park, N. C.; Park, Y. P. Two-dimensional photonic crystal color filter development. *Opt. Express* **2009**, *17*, 8621−8629.
(31) Voges, E. Coupling Techniques: Prism-, Grating- and Endfire-Coupling. In *Integrated Optics: Physics and Applications*; Martellucci, S., Chester, A. N., Eds.; Springer US: Boston, MA, U.S.A., 1983; pp 323−333.
(32) Yeh, A. Y. P. *Photonics: Optical Electronics in Modern Communications*, 6th ed.; Oxford University Press: New York, 2007.
(33) Preston, K.; Schmidt, B.; Lipson, M. Polysilicon photonic resonators for large-scale 3D integration of optical networks. *Opt. Express* **2007**, *15* (25), 17283−1729.
(34) Poon, J. K. S.; Zhu, L.; DeRose, G. A.; Yariv, A. Polymer Microring Coupled-Resonator Optical Waveguides. *J. Lightwave Technol.* **2006**, *24* (4), 1843−1849.

DOI: 10.1021/acsphotonics.8b00022
ACS Photonics 2018, 5, 1839−1845

(35) Seo, B. J.; Kim, S.; Fetterman, H.; Steier, W.; Jin, D.; Dinu, R. Design of ring resonators using electro-optic polymer waveguides. *J. Phys. Chem. C* **2008**, *112*, 7953−7958.
(36) Girault, P.; Lorrain, N.; Poffo, L.; Guendouz, M.; Lemaitre, J.; Carré, C.; Gadonna, M.; Bosc, D.; Vignaud, G. Integrated polymer micro-ring resonators for optical sensing applications. *J. Appl. Phys.* **2015**, *117*, 104504.
(37) Qian, G.; Tang, J.; Zhang, X. Y.; Li, R. Z.; Lu, Y.; Zhang, T. Low-Loss polymer-based ring resonator for resonant integrated optical gyroscopes. *J. Nanomater.* **2014**, *2014*, 119.
(38) Poon, J. K.; Zhu, L.; DeRose, G. A.; Yariv, A. (2006). Polymer microring coupled-resonator optical waveguides. *J. Lightwave Technol.* **2006**, *24*, 1843.
(39) Schell, A. W.; Kaschke, J.; Fischer, J.; Henze, R.; Wolters, J.; Wegener, M.; Benson, O. Three-dimensional quantum photonic elements based on single nitrogen vacancy-centres in laser-written microstructures. *Sci. Rep.* **2013**, *3*, na.

DOI: 10.1021/acsphotonics.8b00022
ACS Photonics 2018, 5, 1839−1845